Check for updates

ASCE

Parametric Programming of 3D Printed Curved Walls for Cost-Efficient Building Design

Alejandro Martínez-Rocamora[1]; Rodrigo García-Alvarado[2]; Euro Casanova-Medina[3]; Luis Felipe González-Böhme[4]; and Fernando Auat-Cheein[5]

Downloaded from ascelibrary.org by Alejandro Martínez Rocamora on 03/01/20. Copyright ASCE. For personal use only; all rights reserved.

Abstract: 3D-printed construction allows elaborating building elements with diverse shapes that are digitally controlled. This paper exposes the modeling of 3D-printed curved walls through parametric programming in building information modeling (BIM) in order to support a cost-efficient building design. The advantage of using curved walls is based on the possibility of reducing their thickness with respect to straight walls of similar length given their higher resistance to overturning forces. The programming developed here can propose a considerable set of solutions using curved walls for a rectangular enclosure of dimensions given by the user. A case study for a vehicle sale pavilion is shown, for which a set of 1,600 solutions with curved walls of different curvature angles and lengths is generated and subsequently analyzed. From this analysis, those models with lower material consumption and execution time are selected to be more thoroughly studied in the design process. Thus, a novel strategy is provided to researchers and practitioners for developing more efficient and expressive building designs based on 3D-printed construction. The most efficient solution identified in the example reduces material consumption by 61%, with an estimated cost saving of 53%. **DOI: 10.1061/(ASCE)CO.1943-7862.0001811.** © *2020 American Society of Civil Engineers.*

Introduction

3D-printed construction is based on the three-dimensional deposition of fast-solidifying fluid compounds, digitally controlled, to build human-scale elements (Bos et al. 2016; Günther et al. 2014; Khoshnevis et al. 2006). Currently, experimentation with this type of construction is being performed in different initiatives around the world using robotic arms and/or gantries that allow the displacement of nozzles connected to concrete—or other mixtures—pumps through a hose to print elements (Doely 2014). In recent years, several examples have been disseminated of small experimental buildings made with 3D-printed construction by entrepreneurs, researchers, and industrial-academic consortiums, such as the Chinese company WinSun (Kira 2015; Levy 2014), Russian company Apis Cor (2018), or Spanish company BeMore3D (2018). Also, ICON and Batiprint have recently presented innovative 3D-printed houses in the United States and France, respectively (ICON 2018; Yhnova 2018).

Most of the studies on 3D-printed construction have focused on exposing and discussing the possibilities of this technology (Bos et al. 2016; Delgado Camacho et al. 2018; Hager et al. 2016; Labonnote et al. 2016; Tay et al. 2017) and on the elaboration of adequate mixtures and singular examples (Keating et al. 2017; Ma and Wang 2017; Martens et al. 2018; Panda et al. 2018). Some recent works have fundamentally tackled the design of architectural elements (Craveiro et al. 2017; Hager et al. 2016; Wolfs 2015) with respect to geometry modeling and the analysis of resistant capacities. Likewise, studies on the material consumption for 3D-printed construction raise new concepts and methods for evaluating the deposition process and the quality of the extruded material (Ma et al. 2018; Malaeb et al. 2015; Wu et al. 2016).

However, the design and management of building elements with this new technology are not covered in the aforementioned studies and experiences. Only a few authors have proposed general classifications of equipment and processes (Bock and Linner 2015); defined machine types and operational attributes for 3D-printed construction (Labonnote et al. 2016); evaluated environmental impact of robotic fabrication (Agustí-Juan et al. 2017); and established ranges of execution according to the size, extrusion, assembly, support and complexity of 3D-printed objects (Duballet et al. 2017). Regarding construction management, Davtalab et al. (2018) proposed a strategy based on graphs to interpret the digital model of a building and determine the printing path for contour crafting machines, although some aspects, such as work volumes or curved elements, were not considered in their study. Existing research shows there is a progression toward establishing general operational definitions for 3D-printed construction. However, the significant novelty of this technology opens a wide research field comprising architectural design, industrialization, and construction management because of the new paradigms of design and construction that it establishes. Among these research gaps, harmonization between the analysis of feasible architectural forms and designs—taking into account the capacities of 3D-printed construction to generate free-form elements—and resource management remains a challenge, for which an interdisciplinary perspective is required. An adequate solution should aim to reduce economic costs, materials consumption, and execution time in the application of this

[1]Assistant Professor, GeDIE Research Group, Dept. of Construction Sciences, Univ. of the Bío-Bío, Concepción 4051381, Chile (corresponding author). ORCID: https://orcid.org/0000-0002-2874-0081. Email: amartinez@ubiobio.cl

[2]Full Professor, GeDIE Research Group, Dept. of Design and Theory of Architecture, Univ. of the Bío-Bío, Concepción 4051381, Chile.

[3]Assistant Professor, GeDIE Research Group, Dept. of Civil and Environmental Engineering, Univ. of the Bío-Bío, Concepción 4051381, Chile. ORCID: https://orcid.org/0000-0002-1701-0550

[4]Assistant Professor, Dept. of Architecture, Technical Univ. Federico Santa María, Valparaíso 2390123, Chile.

[5]Associate Professor, Dept. of Electronic Engineering, Technical Univ. Federico Santa María, Valparaíso 2390123, Chile.

Note. This manuscript was submitted on May 2, 2019; approved on October 11, 2019; published online on February 29, 2020. Discussion period open until July 29, 2020; separate discussions must be submitted for individual papers. This paper is part of the ***Journal of Construction Engineering and Management***, © ASCE, ISSN 0733-9364.

new technology while being automated in accordance with the technological advancement that 3D-printed construction represents.

In order to address this problem, the application of parametric programming is an appropriate tool for the integration of volumetric optimization of curved walls and the evaluation of a considerable set of design alternatives. Specifically, parametric programming is employed here to massively generate a significant set of alternative designs to solve a given enclosure with 3D-printed curved walls, whose higher resistance to overturning forces allows a considerable reduction of their thickness and therefore material consumption. Subsequently, that set of alternative solutions is evaluated based on economic aspects in order to significantly reduce the spectrum of proposals that the designer must finally assess from an aesthetic perspective. Thus, the proposed solution aims to produce resource savings through a massive and automated analysis that allows improved decision-making processes in early design stages, although the underlying concept of the optimization proposal could be applied to numerous other aspects of construction engineering and management.

The following section contains a literature review of 3D-printed construction with concrete, volumetric optimization potential of curved walls, and the use of parametric programming for design in architecture. Then, the calculation of the thickness reduction possibilities of curved walls according to their curvature degree is explained, as well as the visual parametric programming to massively generate solutions for a given space and an initial approach to provide cost evaluation of the studied alternatives. Subsequently, the assessment and discussion of results obtained from the cost analysis is presented. In the final section, some conclusions and future challenges are drawn from this study.

Background

3D-Printed Construction with Concrete

3D-printed construction is currently in the spotlight of the architecture research field mainly because of the numerous advantages it promises, such as construction time and cost savings (Buswell et al. 2007), reduction of waste generation (Lim et al. 2012), and architectural design flexibility. Given its economic, operational, and environmental benefits, robots are expected to play a crucial role in construction in the near future (Bogue 2018).

According to a study focused on the Indian stakeholders perception of 3D-printed construction, Al Abadi et al. (2004) identified the high construction speed as its main advantage, and, in contrast, the lack of documentation, codes, guides, and information in general available among active and emergent professionals as its main weakness. Other authors identified operational-related problems, such as dynamic instabilities, bambooing, nozzle clogging, and overflow, that impede a wider expansion of these construction techniques (Bukkapatnam and Clark 2007).

However, one of the biggest challenges for the development of this field is the determination of cheap, controllable materials with suitable behavior for 3D-printed construction because special mixtures are usually required to obtain the peculiar properties necessary for this type of technology (Barnett and Gosselin 2015; Feng et al. 2015; Le et al. 2012a, b). Generally, this challenge forces the use of concrete, for which it is necessary to manage extrusion and setting times of the mixture between layers, changes in fluidity, and weight to be supported by the machine, implying an exhaustive control of rheology (Weng et al. 2016; Zareiyan and Khoshnevis 2017a; Zareiyan and Khoshnevis 2017b). An interesting advance in the standardization of the newly developed mixtures was presented by Kazemian et al. (2017), who established a framework for laboratory tests on the behavior of cementitious mixtures for 3D-printed construction, defining parameters such as print quality, shape stability, and printability window.

The lack of ductility in the resulting product is added to this challenge. The absence of reinforcements within the concrete mass has frequently limited the use of 3D-printed concrete as formwork for conventional reinforced concrete (Wu et al. 2016), or simply as nonstructural concrete (Gosselin et al. 2016), meaning a waste of the advantages that this technology offers. Other structural issues such as the immediate necessity of load-bearing capacity of uncured concrete to safely erect 3D-printed structures through contour crafting were analyzed by some authors (Di Carlo et al. 2013; Feng et al. 2015; Perrot et al. 2016), achieving structural integrity during free-form fabrication. Also, the inclusion of reinforcement with steel cables during the printing process has been studied by Bos et al. (2018), whereas private companies such as CyBe Construction developed proprietary cement mortars for their prints that set in 3 min and reached structural strength in one hour, as reported by Bogue (2018).

Volumetric Optimization of Curved Walls Subject to Overturning Forces

The stability and overturning behavior of freestanding structures (i.e., structures simply supported by the ground but not attached to it) has received some attention in the literature related to seismic and earthquake engineering. The focus of these works may be classified in three main areas: overturning of storage tanks in industrial facilities (Liu et al. 2016; Shie et al. 2007); stability and rocking behavior of masonry structures (Doherty et al. 2002; Gazetas et al. 2012; Kounadis 2015; Lagomarsino 2015; Peña et al. 2008); and stability of nonstructural objects, such as pieces of art in museums, or equipment components in hospitals and industry (Al Abadi et al. 2004; Berto et al. 2018; Reinoso et al. 2010). All these studies are focused on defining the limit of ground accelerations that a structure can stand before rocking begins or overturning happens to provide design recommendations or to assess the seismic risk of structures already in place. Most of the analyses presented are based on the following hypotheses: the structure is considered a rigid rectangular block or slab and in most cases is symmetric; the friction between the block and the ground is high enough to exclude the effect of sliding; and the ground is assumed rigid.

A freestanding block subject to a constant unidirectional ground acceleration (or applied force) overturns if that acceleration (or force) is greater than a limit value that is a function of the block dimensions and the position of the center of gravity. However, if the ground acceleration is bidirectional, as in a seismic event, the block experiences a rocking motion that might eventually end in overturning. In this case, the rocking response of the block is a function of the slenderness and absolute size of the block (Housner 1963), as well as the amplitude, frequency content, and sequence of pulses of the ground motion (Gazetas et al. 2012).

Only a few of the analyses of structures subject to rocking or overturning consider their shape, and the vast majority only consider flat symmetric blocks. Cylindrical shapes have been studied in the case of storage tanks (Liu et al. 2016; Shie et al. 2007), and an inventory of objects, which most of them are symmetric or axisymmetric (e.g., lamps, blenders, and coffee-pots), has been presented by Reinoso et al. (2010). However, limited work has focused on the overturning criteria for curved blocks or walls.

Downloaded from ascelibrary.org by Alejandro Martínez Rocamora on 03/01/20. Copyright ASCE. For personal use only; all rights reserved.

Parametric Programming in BIM Environments

BIM platforms include visual programming environments for the parametric programming of architectural components. Visual programming allows nonspecialized users who do not have knowledge of programming languages to program simple code in an intuitive way (Lim et al. 2016). Nevertheless, knowledge of advanced coding languages can significantly increase the range of possibilities to develop algorithms to synthetically and automatically construct 3D data to generate complex geometries containing specific properties and information (Gruen et al. 2009; Paoletti 2017), as well as to integrate and relate analysis and decision-making for construction management purposes such as the efficient use of resources.

Most works with parametric programming have focused on developing complex shapes involving algorithmic geometries and fabrication routines (Jabi 2013; Raspall 2015). For example, Griffith and Sass (2006) showed the potential of programming to decompose complex forms such as double-curved walls into constructible forms or pieces, and Cavieres et al. (2011) applied parametric modeling during conceptual design to improve early decision-making, thus proving the possibilities of this technology to embed constructive and structural knowledge in the generation and analysis process. From their study on the geometrically-based generation of curved and sinuous brick walls, they concluded that parametric modeling allows the automation of tedious and error-prone activities and scheduling. Gan et al. (2019) applied topology optimization combined with genetic algorithms for the optimization of costs and carbon emissions of reinforced concrete structures in high-rise buildings, allowing a savings of 18%–24% in embodied carbon and material costs compared to the reference building. Lobaccaro et al. (2018) designed a generative workflow based on parametric design to apply a sequential optimization of a base project regarding solar radiation, daylighting, and environmental impact. This multi-criteria optimization process produced highly unconventional designs that would otherwise remain unexplored.

The possibilities of BIM technologies applied to 3D-printed construction have been extensively indicated (Ma et al. 2018). Davtalab et al. (2018) considered it necessary to integrate robotic construction features in BIM platforms, such as a robot family with operational properties (e.g., speed, acceleration, dimensions, and required voltage) or material specifications (e.g., compressive strength, Young modulus, and density). The inclusion of this information allows designers to perform an early-stage analysis of the suitability of each robot and material to their purposes. This idea was formerly proposed by Correa (2016), who developed a methodology for robot-oriented design in BIM platforms by dividing the model into different parts or pieces based on the work volume of the printer. Also, the possibilities of defining printing paths through parametric programming have been explored and successfully implemented by Lim et al. (2016), as well as work planning based on modular construction (Lee et al. 2019).

In this work, a simple case study consisting of a rectangular enclosure is used for testing the possibilities that parametric programming can offer in integrated design and construction management. Specifically, it is used for performing a constrained analysis of a set of considerable size of alternative designs for a given enclosure solved with 3D-printed curved walls of different curvature and projected length. Therefore, the third feature of the auto-generative design approach is implemented. According to Ostwald (2010), the feature does not produce a singular design solution, but operates by defining a set of conceivable solutions to a design problem, thus producing a constrained continuum of alternatives. The proposal here described provides a combined analysis of resistant capacities and the quantification of resource consumption of design alternatives theoretically built using a novel construction technology, resulting in an innovative approach to integrated management.

Materials and Methods

Thickness Reduction of Curved Walls

Given that 3D-printed construction is currently an emerging technology, there are not many examples of structural elements made of reinforced printed concrete because the necessary resistant capacities to achieve that functionality, as well as operational aspects such as the path followed by the robotic arm to print the element while avoiding the displacement of reinforcement steel bars, still remain as a research challenge (Kreiger et al. 2019). For that reason, in this study, 3D-printed walls are analyzed as nonstructural elements, and the volumetric optimization applied is limited to achieving a specific resistance to overturning using regular curved walls. It is worth noticing that highly optimized designs, such as those offered by topology optimization (Luo et al. 2008), would make the pursued evolution to 3D-printed structural elements less feasible due to the complexity of shaping reinforcement bars to fit highly irregular forms.

Therefore, as the first step in this work, the stability of curved walls is compared to that of straight walls regarding the resistance to overturning to calculate the maximum thickness reduction to resist a similar force. Fig. 1 shows, according to the defined notation, the geometrical parameters involved in this calculation for both curved and straight walls.

The free-body diagrams for curved and straight walls shown in Fig. 2 allow the formulas expressed in Table 1 to be defined, and the table summarizes the calculations for the overturning moment,

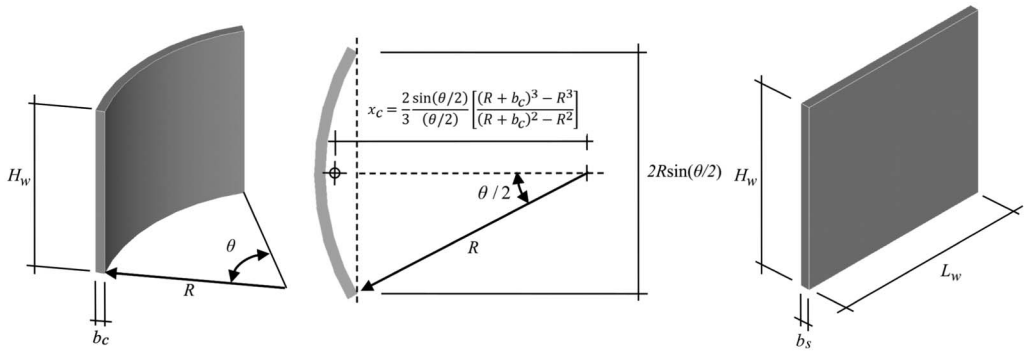

Fig. 1. Geometry of curved and straight walls.

Downloaded from ascelibrary.org by Alejandro Martínez Rocamora on 03/01/20. Copyright ASCE. For personal use only; all rights reserved.

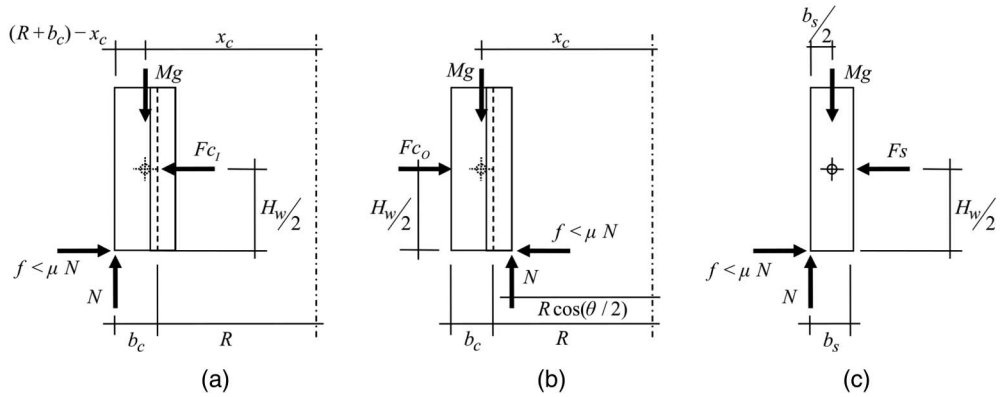

Fig. 2. Free-body diagram for: (a) curved wall (inner force); (b) curved wall (outer force); and (c) straight wall.

Table 1. Overturning forces for curved and straight walls

Wall	Overturning moment	Stabilizing moment	Overturning limit force
Curved (inner force)	$F_{c_I}\frac{H_w}{2}$	$Mg[(R+b_c)-x_c]$	$F_{c_I} \le 2\frac{Mg}{H_w}[(R+b_c)-x_c]$
Curved (outer force)	$F_{c_O}\frac{H_w}{2}$	$Mg[x_c - R\cos(\theta/2)]$	$F_{c_O} \le 2\frac{Mg}{H_w}[R\cos(\theta/2)]$
Straight	$F_s\frac{H_w}{2}$	$Mg\frac{b_s}{2}$	$Fs \le Mg\frac{b_s}{H_w}$

stabilizing moment, and overturning limit forces for curved and straight walls, whether applying forces toward the center of curvature or in the opposite direction. It should be noted here that the resultant of the destabilizing forces F_{c_I}, F_{c_O}, and F_s is vertically located at the medium height of the wall. This position was chosen by considering that, in the case of a seismic event, the resultant of the destabilizing force acts on this location. In addition, it is assumed that the friction factor is high enough to prevent sliding of the walls.

Fig. 3 shows a comparison of overturning forces for a curved wall depending on the direction of the force application. As to be expected, the overturning limit force is always higher when it is applied toward the convex face of the wall (i.e., $F_{c_O} > F_{c_I}$). In other words, curved walls are more stable when forces are applied toward the center of curvature of the wall. For this reason, only the overturning limit force toward the concave face (F_{c_I}) is studied in the following comparisons as the critical case.

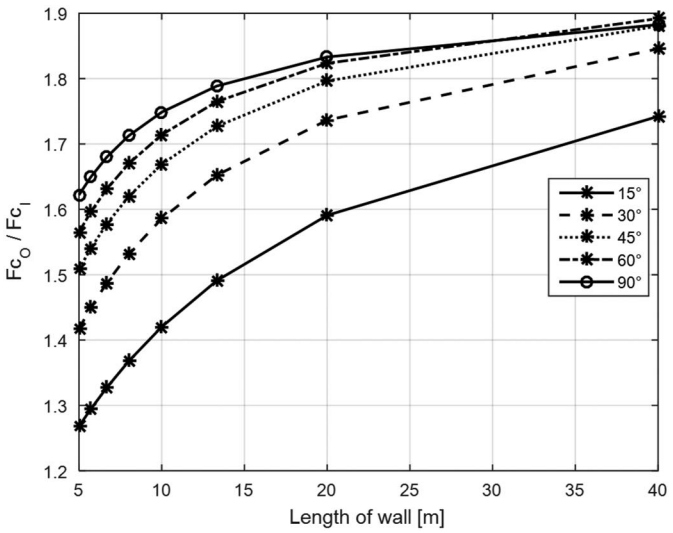

Fig. 3. Comparison of overturning forces for curved walls depending on the direction of the forces.

In this section, the overturning behavior of a curved wall in relation to a straight wall is studied. For this comparison and for all the ensuing cases, the projected length of the curved wall is considered equal to the length of the straight wall in order to have the same enclosure capacity, as expressed in Eq. (1)

$$L_w = 2R\sin(\theta/2) \tag{1}$$

Additionally, to have a fair comparison, the volumes of the straight and curved walls in Eqs. (2) and (3), respectively, are assumed to be equal. Equating both volumes and considering the expression for the wall length shown in Eq. (1) results in Eq. (4), whose solution allows the thickness of the curved wall to be determined as a function of the rest of geometrical parameters

$$V_s = b_s L_w H_w \tag{2}$$

$$V_c = \frac{\theta}{2}(2R + b_c)b_c H_w \tag{3}$$

$$b_c^2 + 2Rb_c - 2Rb_s\frac{\sin(\theta/2)}{(\theta/2)} = 0 \tag{4}$$

Solving Eq. (4) for the angles and projected lengths considered in Fig. 3 allows establishing that the thickness of a curved wall must always be smaller than that of a straight wall with the same projected length because its real length is greater. Fig. 4(a) shows the comparison of the overturning limit forces for a curved (F_{c_I}) and a straight (F_s) wall, assuming the original thickness of the straight wall (b_s) to be 30 cm. This figure shows that for all the angles and projected lengths considered, the overturning limit force is always

J. Constr. Eng. Manage., 2020, 146(5): 04020039

Downloaded from ascelibrary.org by Alejandro Martínez Rocamora on 03/01/20. Copyright ASCE. For personal use only; all rights reserved.

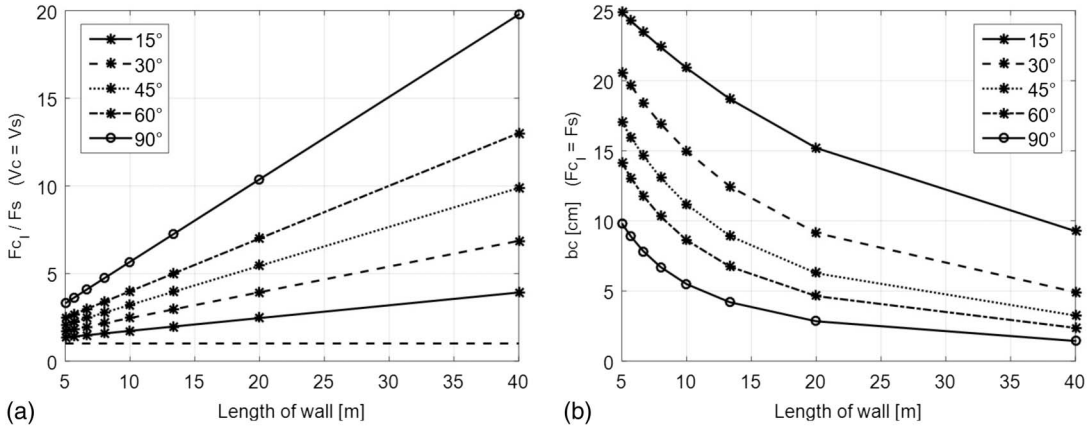

Fig. 4. (a) Overturning limit forces for curved and straight walls with the same projected length and volume; and (b) thickness of curved walls with the same overturning limit forces than a straight wall 30 cm thick with the same projected length and height.

greater for a curved wall than for a straight wall. In other words, the curved wall is always more stable than the equivalent straight wall (i.e., with the same projected length and volume). Based on this observation, a reduced thickness for the curved wall may be calculated to resist the same overturning limit force than that of the equivalent straight wall (i.e., $F_s = F_{c_l}$). This condition translates into the following nonlinear equation [Eq. (5)], whose results of the significant reductions of the curved wall thickness (b_c) that may be attained are shown in Fig. 4(b)

$$\theta(2R + b_c)b_c\left\{(R + b_c) - \frac{2}{3}\frac{\sin(\theta/2)}{(\theta/2)}\left[\frac{(R + b_c)^3 - R^3}{(R + b_c)^2 - R^2}\right]\right\} - 2Rb_s^2\sin(\theta/2) = 0 \quad (5)$$

As an application example of the previously defined equations, Table 2 shows the potential reductions of the thickness (b_c) and volume (V_c) of curved walls that resist the same overturning force as a straight wall 2.5 m high and 30 cm thick when considering certain variations of its projected length and curvature angle to resist. Overturning limit forces are presented relative to the specific weight of the material ($\gamma = \rho g$), where ρ is the material density, in order to make values independent of the construction material chosen. It is worth mentioning that finite element simulations were performed for the cases included therein, where it was determined that the theoretical approach used in these calculations becomes less valid when the wall's arc-length increases significantly, i.e., when either the curvature angle or the projected length attains the maximum values considered. Therefore, it was decided to apply a constraint to require a minimum thickness of 7 cm, thus discarding the values in gray in Table 2. Also, the collaboration between consecutive curved walls has not been calculated, but it would likely allow a larger decrease of the necessary thickness to resist the same overturning force.

To prepare for the next step of the study, where the parametric programming must assign the appropriate thickness for each curved wall, a BIM file was configured with a family containing 30 different types of 3D-printed concrete walls. These types are identified by their thicknesses (b_c), and they vary according to the results from Eq. (5) rounded up to the next integer value in centimeters.

Massive Generation of Constrained Parametric Designs of Alternative Solutions

As an initial approach to this problem, a 40×40 matrix of alternative solutions for a rectangular enclosure with curved walls was generated and analyzed through parametric programming, considering that the study of this significant amount of solutions with such similarity in their appearance would be extremely difficult in a traditional design process (Martabid and Mourgues 2015). The size of

Table 2. Results summary of thickness and volume for curved walls with overturning forces resistance equivalent to that of a straight wall ($b_s = 30$ cm, $H_w = 2.5$ m)

		Projected length of the wall, w (m)							
Wall	Parameter	5.00	5.71	6.67	8.00	10.00	13.33	20.00	40.00
Straight	b_r (cm)	30.00	30.00	30.00	30.00	30.00	30.00	30.00	30.00
	V_r (m^3)	3.75	4.28	5.00	6.00	7.50	9.99	15.00	30.00
	F_s/γ (m^3)	0.45	0.51	0.60	0.72	0.90	1.20	1.80	3.60
$\theta = 15°$	b_c (cm)	24.88	24.27	23.46	22.40	20.91	18.71	15.21	9.27
Curved	V_c (m^3)	3.14	3.49	3.94	4.51	5.26	6.26	7.63	9.30
$\theta = 30°$	b_c (cm)	20.59	19.63	18.43	16.93	14.99	12.46	9.14	4.92
Curved	V_c (m^3)	2.63	2.86	3.13	3.44	3.81	4.21	4.63	4.97
$\theta = 45°$	b_c (cm)	17.06	15.96	14.64	13.07	11.18	8.93	6.27	3.25
Curved	V_c (m^3)	2.22	2.36	2.53	2.70	2.88	3.06	3.22	3.33
$\theta = 60°$	b_c (cm)	14.17	13.06	11.77	10.31	8.63	6.74	4.64	2.37
Curved	V_c (m^3)	1.88	1.97	2.07	2.17	2.27	2.36	2.43	2.48
$\theta = 90°$	b_c (cm)	9.83	8.88	7.83	6.70	5.49	4.20	2.84	1.43
Curved	V_c (m^3)	1.38	1.42	1.46	1.50	1.53	1.56	1.58	1.59

Downloaded from ascelibrary.org by Alejandro Martínez Rocamora on 03/01/20. Copyright ASCE. For personal use only; all rights reserved.

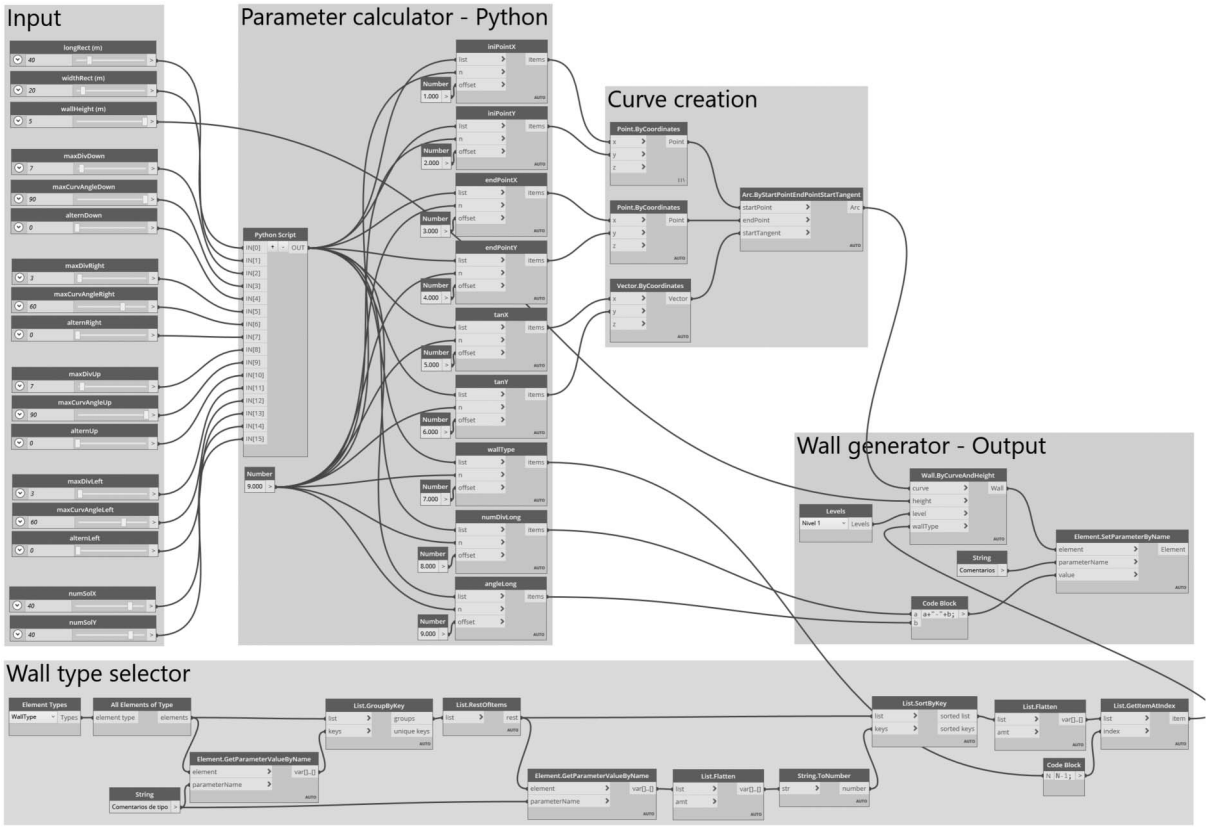

Fig. 5. Blocks of visual programming for the generation of multiple alternatives of the enclosure using curved walls.

the matrix chosen here was conditioned by processing and memory limitations of the computer equipment used to generate it, but these dimensions have been left as configurable parameters, thus allowing users to control the number of alternatives to be generated.

The automatic generation of alternatives is performed by parametric programming using the visual programming environment available in Autodesk Revit, called Dynamo. The Dynamo scheme consists of five main blocks, starting with an initial input (Fig. 5) containing the following input variables, which are to be configured by the user:

- $numSolX$ and $numSolY$: size of the solutions matrix.
- $longRect$ and $widthRect$: dimensions of the rectangle to be solved [m].
- $wallHeight$: height of the enclosure's wall [m].
- $maxDiv_i$, $maxCurvAngle_i$: maximum number of divisions and curvature angle of side i
- $altern_i$: alternation mode of side i (0 = random, 1 = outer arcs, 2 = inner arcs, 3 = alternating).

The parameter calculator block is in charge of the treatment of input data to determine the necessary parameters for generating walls from curves (e.g., initial point, end point, and tangent value) and their characterization with a codification that allows the subsequent quantification of each solution's length and volume and the assessment of results. This block contains an internal Python code to simplify the parameterization of curved walls because developing that code in visual programming would need a huge amount of blocks and connectors that would make the algorithm more difficult to understand.

Inside the Python code block, the determination of the parameters to draw each curved wall is implemented according to the flowchart shown in Fig. 6. The function first receives the input data (step 1) and goes over each alternative solution (outer loop), determining the coordinates of the base point to be used for the current solution (step 2). Then, it loops over each of its sides (mid loop), randomizing the number of sections into which they will be divided in integer values from 1 to the value of the $maxDiv_i$ variable defined by the user, and calculating the projected length of each section (step 3). Finally, for each section of the current side (inner loop), its curvature angle is randomized from 1 to the value of the $maxCurvAngle_i$ variable (step 4). This randomization of the curvature angle of each arc directly affects the total length of the current solution and therefore the time needed for the execution of its layers using 3D-printed construction.

Based on the previously determined parameters, the algorithm first obtains the initial and final points for the current arc (step 5). Then, it calculates the curvature radio and applies Eq. (5) to obtain the lowest thickness possible for the corresponding curved wall to resist an equivalent overturning force and therefore the wall type to be selected (step 6). As was mentioned previously, an internal constraint was applied regarding constructive feasibility, not allowing the use of thicknesses below 7 cm. Finally, the angle and tangent to be used for the generation of the current arc are geometrically calculated (step 7), and the complete set of parameters that define the current arc is added to the output array (step 8).

In the next step of the visual programming (see curve creation block in Fig. 6), the data calculated for the initial point, final point, and tangent value are retrieved to create the arcs that serve as a basis to build the curved walls. In parallel, the wall type selector block first filters the available wall types in the BIM model to obtain a sorted list with the 30 wall types defined. Then, it receives from the parameter calculator block the wall type to be assigned to the current curved wall and selects it from the list. The assignation of the appropriate wall type directly affects the volume of the solution due

Downloaded from ascelibrary.org by Alejandro Martínez Rocamora on 03/01/20. Copyright ASCE. For personal use only; all rights reserved.

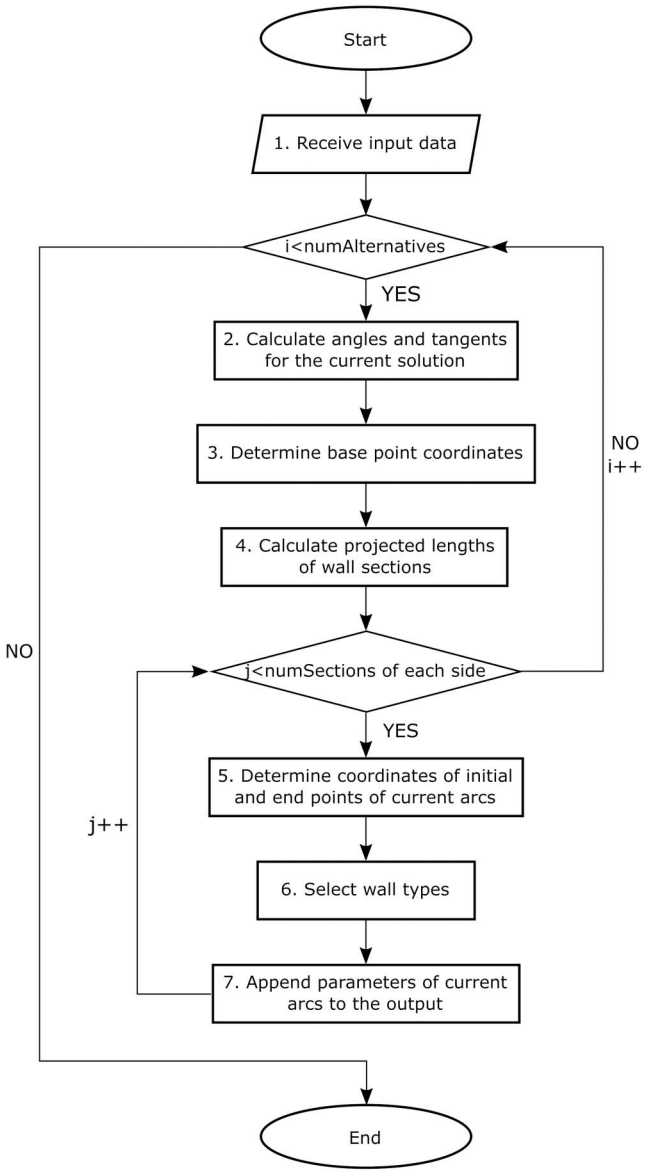

Fig. 6. Flowchart of the Python module for determining the necessary parameters for the creation of curves and their respective walls.

to variations in its thickness parameter and, as a consequence, its material consumption and economic cost.

Finally, the wall generator block receives from the curve creation block the base arc upon which the current wall section must be built, the wall type from the wall type selector block, the wall's height from the input block, and the parameters for the characterization of the solution to which the current wall section belongs from the parameter calculator block. Each curved wall is characterized through the Comments instance parameter as a code in the form X-Y, where X and Y correspond to the coordinates in the matrix of the solution to which the wall section belongs to ease its identification.

Once the described parametric program has been executed, a quantification schedule grouped by the value of the Comments parameter is built, and the total length and volume are obtained for each solution, which are key factors in the assessment of results in the next section. In this analysis, Eq. (6) is proposed as a first approach to objectively compare the various solutions in economic terms by breaking down the 3D-printing activity into materials, machinery, and manpower needs, which is similar to the classic methods for the calculation of unitary costs in the construction management field:

$$C_{sol} = \left(L_e \cdot \frac{H_w}{H_l}/S_{mc}\right) \cdot \left(\frac{C_{mc}}{SL_{mc}} + C_{op}\right) + V_{mt} \cdot C_{mt} \qquad (6)$$

where all the parameters considered are included in the notation and are to be configured by the user except for the total length and volume of each solution, which are given by the results from the previous algorithm.

The two following simplification/simplifying (whichever is more correct) assumptions are considered:

- The time for changing the position of the printing machine or robot to print the wall is omitted, thereby assuming a continuous system by means of a large installation and/or multi-robot coordination to cover the entire construction.
- The printing machine can adjust the thickness through the extrusion speed and nozzle size during the printing process. Therefore, printing one meter of a layer takes the same amount of time for any thickness of the wall.

Furthermore, the economic analysis does not consider differences in the built-up surface of each solution produced by the concave or convex curvature of the walls, although this limitation is highlighted in the conclusions as a possible improvement in forthcoming advances of this research.

Results and Discussion

The described parametric procedure is applied to a case study of a triangular 5,000 m^2 lot destined for an auto dealer located in a main avenue in Concepción, Chile (Fig. 7). The pavilion planned for the front section of the lot requires an enclosure with a unique open space of approximately 800 m^2 and 5 m height to accommodate a dozen vehicles and two attention desks, assuming other services, offices, and workshops will be allocated in another building. According to the designer, the pavilion must consider a rectangular volume with a dynamic aspect appropriate for a sports car brand. Therefore, its short sides should have up to three soft-curved (60°) wall segments in order to host more regular functions, while its long sides should consider up to seven segments with greater curvature angles (90°) to support different car exhibitions both indoors and outdoors and to allow more variations on each lateral view from the avenue. The direction of each curved wall is to be left as a random parameter in order to increase the variability of the generated solutions. The massive analysis of hundreds of alternative solutions considering the previous aspects is required to support the conventional capacities of designers, who are usually able to review dozens of variations through manual design or digital repetitions, both taking several working hours.

The application of the previously described parametric procedure to this case study first generated a 40 × 40 matrix of different solutions with curved walls for the same 40 × 20 m rectangular enclosure (Fig. 8). Then, the volume and length were determined for each alternative solution through quantification tables and transformed to economic cost using Eq. (6). For this case study, an average cost of 125,000 USD and service life of 90,000 h were assumed for an industrial robotic arm including peripherals, and an hourly cost of 80 USD/h were assigned for the specialized operator (Agustí-Juan et al. 2017; García de Soto et al. 2018). Also, an average cost of 168 USD/m^3 was used for concrete placed on site, with an increase of 20% over market costs due to the special characteristics needed for 3D-printing concrete (Cobod 2019). The heights of walls and layers were set to 5 m and 3 cm, respectively, thus

Downloaded from ascelibrary.org by Alejandro Martínez Rocamora on 03/01/20. Copyright ASCE. For personal use only; all rights reserved.

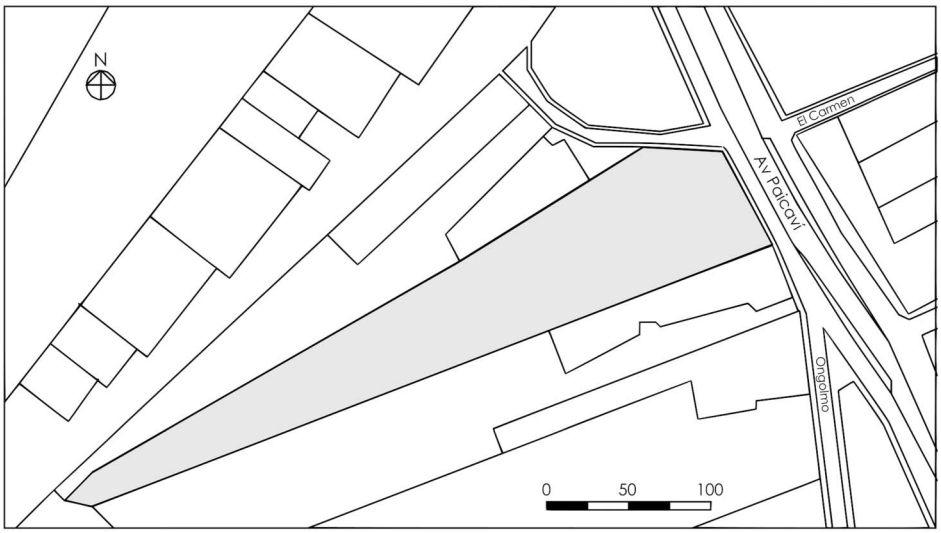

Fig. 7. Site view of the case study in Concepción (Chile).

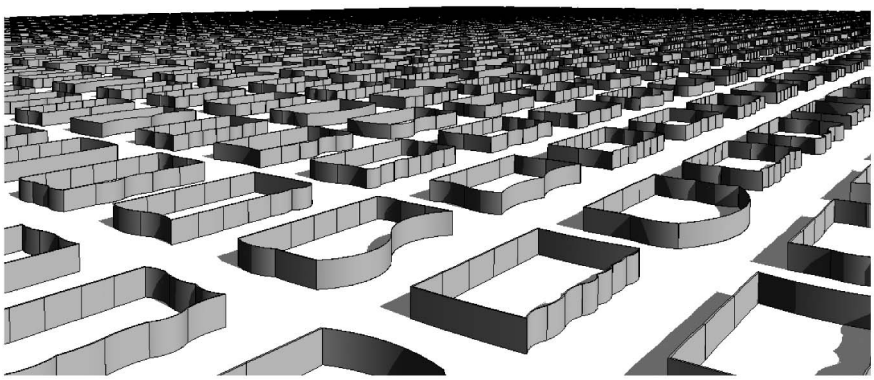

Fig. 8. Automatically generated 1,600 alternatives using curved walls to solve the 40 × 20 m enclosure of the case study.

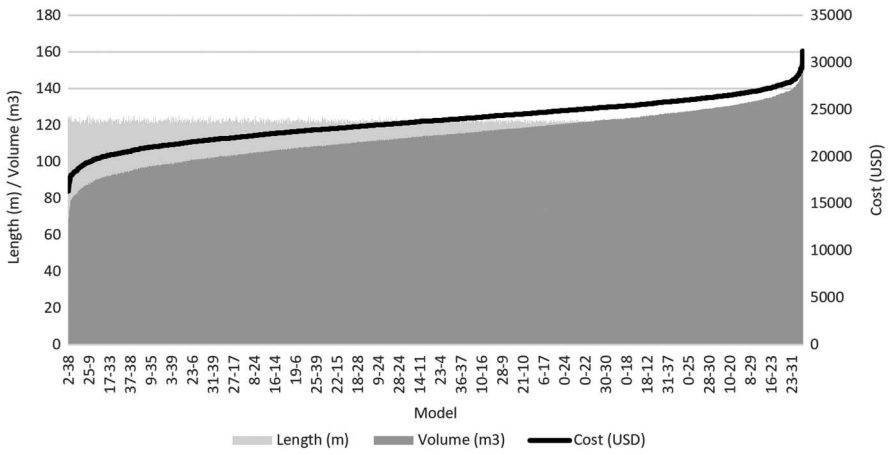

Fig. 9. Economic comparison of 1,600 design alternatives complying with the 7 cm thickness constraint.

needing 167 layers to complete a wall, and the printing speed was set to a minimum of 6 m/min, as suggested by Cobod (2019). The wall length and volume of material were obtained directly from the quantification tables within the BIM model in which the solutions were generated. For the example of execution shown in this section, a total of 19,153 arcs were defined to form the 1,600 solutions, but given the randomness of the algorithm, the number of arcs varies in each execution.

The assessment of the results from the massive generation algorithm reveals that Eq. (6) is much more sensitive to changes

Downloaded from ascelibrary.org by Alejandro Martínez Rocamora on 03/01/20. Copyright ASCE. For personal use only; all rights reserved.

in the volume of material than to the total length of the solution (i.e., execution time) since solutions with the lowest material consumption coincide with the cheapest ones (Fig. 9). In contrast, the shortest alternative is any solution that applies the smallest curvature angles in its arcs, disregarding the number of sections into which each side is divided.

Subsequently, those designs that required less material consumption, execution time, and cost were identified to form a

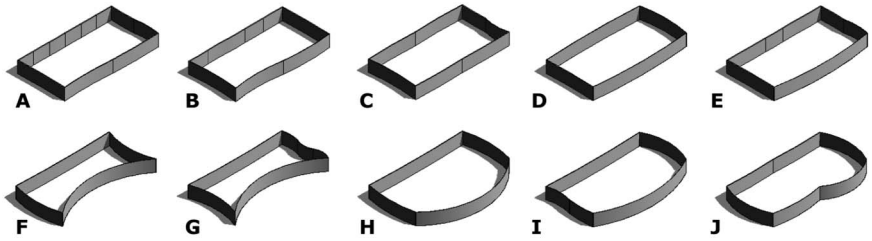

Fig. 10. Aerial renders of the best solutions in terms of (a–e) execution time; and (f–j) material consumption and economic cost.

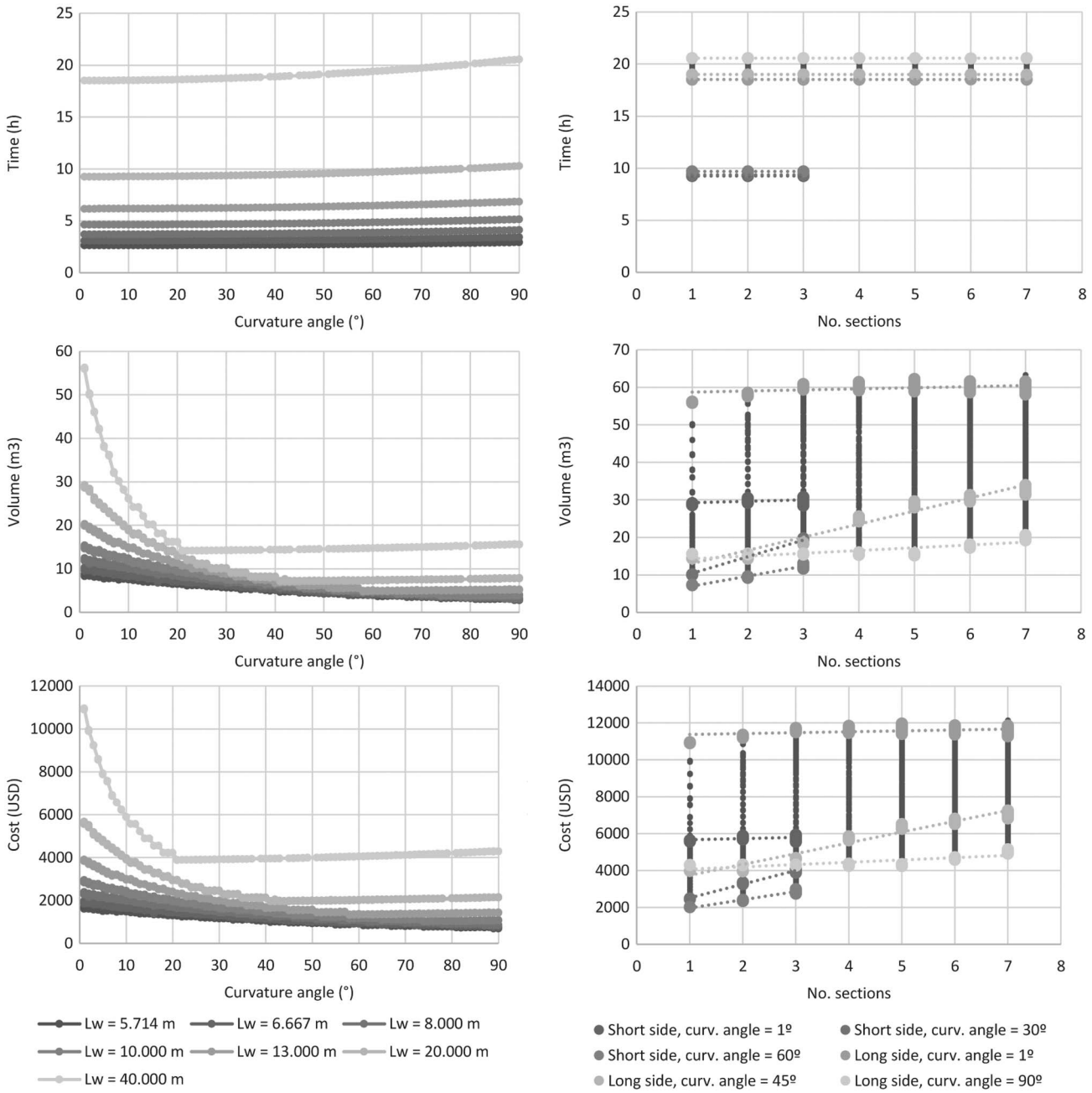

Fig. 11. Analysis of relationships between input and output variables.

J. Constr. Eng. Manage., 2020, 146(5): 04020039

Downloaded from ascelibrary.org by Alejandro Martínez Rocamora on 03/01/20. Copyright ASCE. For personal use only; all rights reserved.

selection of the best solutions among which the designer must make a decision. In this example, the best solution in terms of printing speed [Fig. 10(a)] had a wall length of 120.13 m with soft curves in all its sides. Considering layers 3 cm thick and walls with a height of 5 m, the total length in this case was 20,022 m, which could be printed in 55.62 h if a printing speed of 6 m per minute was applied. Taking into account the set of assumptions established in this study, this solution would only take 4.2 extra minutes to be printed when compared to the base case study, while providing some dynamic variations to its design, a 17.7% reduction of material consumption, and cost savings of 15.4%. The most cost-efficient solution had one single arc on each side, and one of them had a significant curvature angle [Fig. 10(f)] that translated in the lowest material consumption of all the alternatives, with 69.45 m^3 and an estimated economic cost of 16,342 USD, representing 61.4% material and 53% cost savings when compared to the base case study. Although the applied calculation is presented as the first approach with limited accuracy, the figures show that a considerable reduction of material consumption and costs can be achieved through the use of thinner curved walls instead of traditional architectural designs.

The selection of the most efficient solutions in terms of printing time [Figs. 10(a–e)], material consumption and economic cost [Figs. 10(f–j)] includes a variety of architectural forms with significant asymmetries, showing a general tendency to long curved sections and a minor presence of more fragmented configurations. For example, models F and G reduce the interior surface in exchange for bigger exterior support for the exhibition of vehicles, while others increase the interior volume (H–J). Through the described process, an improved decision-making method is thereby achieved, where aerial or ground views of the most efficient models selected from a massive generation of alternatives are presented for the designer's consideration and architectural analysis. This selection also exhibits significant spatial and aesthetic differences, thus expanding the possibilities of architectural design.

An analysis of the correlation existing between the randomized input variables (number of sections for each side, and curvature angle for each curved wall) and the output variables (time, volume, and cost) was performed in order to identify recommendations for improving efficiency regarding these three factors (Fig. 11). To that end, the 19,153 curved walls generated in this execution of the algorithm were used as observations, blocking the confounding variables for each input (see legend in each column of Fig. 11).

From this analysis, the correlation between cost and volume observed in Fig. 9 can be confirmed, since both charts follow a similar pattern, while time remains less related. Additionally, no correlation was identified between the number of sections and any of the output variables because they had significantly low coefficient of determination values. In contrast, the correlation between the curvature angle and the execution time followed a parabolic curve with considerably low values of the variable terms. This reflects a slow increase of time when the curvature angle increases, and this is logical since for a same projected length, and given the assumptions of this study regarding the adaptable size of the nozzle, a greater curvature angle makes the wall longer and therefore more time is needed for its 3D-printing.

A more significant correlation was identified between the curvature angle and the volume and cost. In this case, the charts follow an exponential curve with a value of the coefficient of determination higher than 0.99. However, two peculiarities occur that are highly related to the assumptions in this study. First, a step effect can be observed in each series due to the use of integer values of walls' thicknesses (in centimeters), making the volume and cost increase with the curvature angle, while the calculations do not allow the reduction to the next lower thickness. Second, each series follows the exponential curve until it reaches a limit and then follows a linear increase. This limit is given by the thickness constraint applied in this study, making the walls increase their volume and cost when the curvature angle (and therefore their length) increases because they cannot longer reduce their thickness.

These findings indicate that the recommended strategy for optimizing material consumption and costs would be to increase the curvature angle of walls until they reach the minimum possible volume allowed by the thickness constraint. If the aim is to reduce the execution time, the designer should use lower curvature angles, and this finding is highly influenced by the aforementioned assumption regarding the adaptable size of the nozzle. Therefore, forthcoming advances of this research should focus on the influence of a limited nozzle size when the wall's thickness is greater, thus forcing the 3D-printing process to consider several cords to print each layer of the wall.

Conclusions

In this paper, a methodology is presented for the integration of parametric programming and optimal evaluation of architectural design alternatives that exploit the benefits of 3D-printing technologies. Specifically, a construction cost evaluation of different designs using curved walls was implemented based on their possibility of using a smaller thickness for an equivalent overturning resistance than straight walls.

The parametric programming was implemented in Dynamo, and the possibility of including complex mathematical constraints (e.g., nonlinear equations) and specific criteria based constraints (e.g., wall thickness greater than certain specific value) was shown and applied to a specific design problem. This parametric programming provides the capacity to generate and analyze huge sets of architectural designs at a speed significantly higher than that of humans, thus becoming a useful tool for supporting efficient and diverse design of buildings using 3D-printed construction, as well as for the rapid study of a massive amount of alternative solutions during early-stages of the architectural design process. While the efficiency assessment of the generated alternatives can be performed internally and show only the most efficient solution, one of the main interests of the programming presented here is in the pause implemented in the process in order to show all the alternatives together. Given the randomness of this process, this pause allows the great diversity and heterogeneity of the generated designs to be observed, thus highlighting the superiority of the assessment capacity of the algorithm compared to that of a practitioner who would need to analyze each alternative one at a time.

The particular characteristics of 3D-printed construction technology allow the fabrication of curved walls more easily than traditional construction techniques. This provides greater stability to overturning forces; consequently, a considerable reduction of the necessary thickness of these walls can be achieved, having a significant impact on material consumption, execution time, and therefore economic cost. This reduction could be greater than calculated in this study because collaboration between adjacent wall sections would improve their resistance to overturning. Also, the resistance of walls was studied without considering the benefits of reinforcing steel, while its inclusion into 3D-printed concrete elements still remains a research challenge.

In this article, constraints and optimization were based on the thickness of walls and their construction cost, respectively. However, the link of parametric programming with 3D-printed construction offers the possibility of including constraints and criteria to

Downloaded from ascelibrary.org by Alejandro Martínez Rocamora on 03/01/20. Copyright ASCE. For personal use only; all rights reserved.

drive the generation and evaluation of architectural designs. Even more sophisticated evaluations, like finite element analysis of the structure or thermal behavior, may be incorporated once the parametric model is available. This combination also enables the incorporation of artificial intelligence and machine-learning algorithms to the design process in order to refine the selection of alternatives through the application of additional requirements. Nevertheless, the application of the proposed methodology clearly shows that important cost reductions can be achieved by employing curved walls. The generation process may be as random as desired by the designer since the automatic evaluation ranks the solutions according to a predefined criterion, which translates in a subset of optimal solutions that can be assessed by designers purely regarding their architectural merit.

Forthcoming research is expected to focus on the sequence of necessary positions of a robotic arm to execute a building layout according to its design and the machine's range since the time for machine re-positioning can considerably influence the execution time and, as a consequence, the economic cost of the studied solutions. Thus, architectural designs could be reversely generated and evaluated according to the 3D-printing machines used. Also, the economic analysis of built-up surface differences in the designs produced by the use of concave or convex curvature for the walls should be included in future advances of the methodology proposed in this work.

Data Availability Statement

Some or all data, models, or code generated or used during the study are available from the corresponding author by request and in the Supplemental Data to this article. The available data items are the following:

- A Dynamo Revit 2.0 file with the parametric programming described in this article.
- An empty Revit 2019 model prepared for the execution of the Dynamo file.

Acknowledgments

The authors gratefully acknowledge the National Commission for Science and Technology Research in Chile (CONICYT) for funding this research under Grant FONDECYT 1181015 and Grant Basal FB0008.

Notation

The following symbols are used in this paper:

b = thickness of the curved (b_c) or straight (b_s) wall (m);
C_{mc} = total cost of the printing machine (USD);
C_{mt} = cost of the printing material (USD/m^3);
C_{op} = hourly cost of the operator (USD/h);
C_{sol} = total cost of the evaluated solution (USD);
f = frictional force (N);
F_{c_I} = overturning limit force applied toward the concave face of the curved wall (N);
F_{c_O} = overturning limit force applied toward the convex face of the curved wall (N);
F_s = overturning limit force for a straight wall;
g = gravity value (m/s^2);
H_l = height of each printed layer (m);
H_w = height of the wall (m);
L_e = total length of the enclosure (m);
L_w = projected length of the wall (m);
M = mass of the wall (kg);
N = normal force (N);
R = curvature radius of the curved wall (m);
S_{mc} = printing speed of the machine (m/h);
SL_{mc} = service life of the printing machine (h);
V = volume of the curved (V_c) or straight (V_s) wall (m^3);
V_{mt} = total volume of material consumed for building the walls (m^3);
x_c = centroid of the curved wall (measured from the curvature center of the wall) (m);
γ = specific weight of the material (kg/m^{2}s^2);
μ = friction coefficient (adimensional); and
ρ = density of the material (kg/m^3).

Supplemental Data

A Dynamo file with parametric programming and an empty Revit model prepared for its execution are available online in the ASCE Library (www.ascelibrary.org).

References

Agustí-Juan, I., F. Müller, N. Hack, T. Wangler, and G. Habert. 2017. "Potential benefits of digital fabrication for complex structures: Environmental assessment of a robotically fabricated concrete wall." *J. Clean. Prod.* 154 (Jun): 330–340. https://doi.org/10.1016/j.jclepro.2017.04.002.

Al Abadi, H., N. T. K. Lam, E. Gad, and A. M. Chandler. 2004. "Modelling of earthquake induced overturning of building contents." In *Proc., Australian Earthquake Engineering Society Annual Technical Conf.*, 10.1–10.6. Mt. Gambier, SA: Australian Earthquake Engineering Society.

Apis Cor. 2018. "Apis cor website." Accessed January 20, 2019. http://apis-cor.com/en/.

Barnett, E., and C. Gosselin. 2015. "Large-scale 3D printing with a cable-suspended robot." *Addit. Manuf.* 7 (Jul): 27–44. https://doi.org/10.1016/j.addma.2015.05.001.

BeMore3D. 2018. "Bemore3D website." Accessed February 15, 2019. http://bemore3d.com/.

Berto, L., I. Rocca, and A. Saetta. 2018. "Vulnerability assessment methods for rocking and overturning of free standing elements." *Soil Dyn. Earthquake Eng.* 110 (Jul): 121–136. https://doi.org/10.1016/j.soildyn.2018.02.010.

Bock, T., and T. Linner. 2015. *Robot-oriented design: Design and management tools for the deployment of automation and robotics in construction*. 1st ed. New York: Cambridge University Press.

Bogue, R. 2018. "What are the prospects for robots in the construction industry?" *Ind. Robot* 45 (1): 1–6. https://doi.org/10.1108/IR-11-2017-0194.

Bos, F., Z. Ahmed, R. Wolfs, and T. Salet. 2018. "3D printing concrete with reinforcement." In Vol. 1 of *High tech concrete: Where technology and engineering meet*. Cham, Switzerland: Springer.

Bos, F., R. Wolfs, Z. Ahmed, and T. Salet. 2016. "Additive manufacturing of concrete in construction: Potentials and challenges of 3D concrete printing." *Virtual Phys. Prototyping* 11 (3): 209–225. https://doi.org/10.1080/17452759.2016.1209867.

Bukkapatnam, S., and B. Clark. 2007. "Dynamic modeling and monitoring of contour crafting—An extrusion-based layered manufacturing process." *J. Manuf. Sci. Eng.* 129 (1): 135. https://doi.org/10.1115/1.2375137.

Buswell, R., R. Soar, A. Gibb, and A. Thorpe. 2007. "Freeform construction: Mega-scale rapid manufacturing for construction." *Autom. Constr.* 16 (2): 224–231. https://doi.org/10.1016/j.autcon.2006.05.002.

Downloaded from ascelibrary.org by Alejandro Martínez Rocamora on 03/01/20. Copyright ASCE. For personal use only; all rights reserved.

Cavieres, A., R. Gentry, and T. Al-Haddad. 2011. "Knowledge-based parametric tools for concrete masonry walls: Conceptual design and preliminary structural analysis." *Autom. Constr.* 20 (6): 716–728. https://doi.org/10.1016/j.autcon.2011.01.003.

Cobod. 2019. "3D construction wall printing calculator." Accessed February 27, 2019. http://cobod.com/project-cost-calculator/.

Correa, F. 2016. "Robot-oriented design for production in the context of building information modeling." In *Proc., 33rd Int. Symp. on Automation and Robotics in Construction, ISARC 2016*, 853–861. Oulu, Finland: International Association for Automation and Robotics in Construction.

Craveiro, F., H. Bartolo, A. Gale, J. Duarte, and P. Bartolo. 2017. "A design tool for resource-efficient fabrication of 3D-graded structural building components using additive manufacturing." *Autom. Constr.* 82 (Oct): 75–83. https://doi.org/10.1016/j.autcon.2017.05.006.

Davtalab, O., A. Kazemian, and B. Khoshnevis. 2018. "Perspectives on a bim-integrated software platform for robotic construction through contour crafting." *Autom. Constr.* 89 (May): 13–23. https://doi.org/10.1016/j.autcon.2018.01.006.

Delgado Camacho, D., P. Clayton, W. O'Brien, C. Seepersad, M. Juenger, R. Ferron, and S. Salamone. 2018. "Applications of additive manufacturing in the construction industry—A forward-looking review." *Autom. Constr.* 89 (May): 110–119. https://doi.org/10.1016/j.autcon.2017.12.031.

Di Carlo, T., B. Khoshnevis, and Y. Chen. 2013. "Manufacturing additively, with fresh concrete." In *Proc., IMECE2013—Int. Mechanical Engineering Congress and Exposition*, 1–9. New York: ASME.

Doely, P. 2014. "3D printing: A new dimension in construction." Accessed March 17, 2019. http://fwhtlaw.com/briefing-papers/3d-printing-new-dimension-construction/.

Doherty, K., M. Griffith, N. Lam, and J. Wilson. 2002. "Displacement-based seismic analysis for out-of-plane bending of unreinforced masonry walls." *Earthquake Eng. Struct. D.* 31 (4): 833–850. https://doi.org/10.1002/eqe.126.

Duballet, R., O. Baverel, and J. Dirrenberger. 2017. "Classification of building systems for concrete 3D printing." *Autom. Constr.* 83 (Nov): 247–258. https://doi.org/10.1016/j.autcon.2017.08.018.

Feng, P., X. Meng, J.-F. Chen, and L. Ye. 2015. "Mechanical properties of structures 3D printed with cementitious powders." *Constr. Build. Mater.* 93 (Sep): 486–497. https://doi.org/10.1016/j.conbuildmat.2015.05.132.

Gan, V., C. Wong, K. Tse, J. Cheng, I. Lo, and C. Chan. 2019. "Parametric modelling and evolutionary optimization for cost-optimal and low-carbon design of high-rise reinforced concrete buildings." *Adv. Eng. Inf.* 42 (Oct): 100962. https://doi.org/10.1016/j.aei.2019.100962.

García de Soto, B., I. Agustí-Juan, J. Hunhevicz, S. Joss, K. Graser, G. Habert, and B. Adey. 2018. "Productivity of digital fabrication in construction: Cost and time analysis of a robotically built wall." *Autom. Constr.* 92 (Aug): 297–311. https://doi.org/10.1016/j.autcon.2018.04.004.

Gazetas, G., E. Garini, J. Berrill, and M. Apostolou. 2012. "Sliding and overturning potential of Christchurch 2011 earthquake records." *Earthquake Eng. Struct. D.* 41 (14): 1921–1944. https://doi.org/10.1002/eqe.2165.

Gosselin, C., R. Duballet, P. Roux, N. Gaudillière, J. Dirrenberger, and P. Morel. 2016. "Large-scale 3D printing of ultra-high performance concrete—A new processing route for architects and builders." *Mater. Des.* 100 (Jun): 102–109. https://doi.org/10.1016/j.matdes.2016.03.097.

Griffith, K., and L. Sass. 2006. "Computing and materializing non-uniform shapes: An evolutionary approach to generate and digitally fabricate non-uniform masonry walls." In *Proc., 11th Int. Conf. on Computer Aided Architectural Design Research in Asia: CAADRIA 2006*, 227–235. Kumamoto, Japan: Kumamoto Univ.

Gruen, A., M. Behnisch, and N. Kohler. 2009. "Perspectives in the reality-based generation, nD modelling, and operation of buildings and building stocks." *Build. Res. Inf.* 37 (5–6): 503–519. https://doi.org/10.1080/09613210903189509.

Günther, D., B. Heymel, J. Franz Günther, and I. Ederer. 2014. "Continuous 3D-printing for additive manufacturing." *Rapid Prototyping J.* 20 (4): 320–327. https://doi.org/10.1108/RPJ-08-2012-0068.

Hager, I., A. Golonka, and R. Putanowicz. 2016. "3D printing of buildings and building components as the future of sustainable construction?" *Procedia Eng.* 151: 292–299. https://doi.org/10.1016/j.proeng.2016.07.357.

Housner, G. 1963. "The behavior of inverted pendulum structures during earthquakes." *Bull. Seismol. Soc. Am.* 53 (2): 403–417.

ICON. 2018. "Icon partnered with the non-profit new story to build the first permitted, 3D-printed home in America." Accessed March 17, 2019. https://www.iconbuild.com/new-story.

Jabi, W. 2013. *Parametric design for architecture*. 1st ed. London: Laurence King.

Kazemian, A., X. Yuan, E. Cochran, and B. Khoshnevis. 2017. "Cementitious materials for construction-scale 3D printing: Laboratory testing of fresh printing mixture." *Constr. Build. Mater.* 145 (Aug): 639–647. https://doi.org/10.1016/j.conbuildmat.2017.04.015.

Keating, S., J. Leland, L. Cai, and N. Oxman. 2017. "Toward site-specific and self-sufficient robotic fabrication on architectural scales." *Sci. Robot.* 2 (5): eaam8986. https://doi.org/10.1126/scirobotics.aam8986.

Khoshnevis, B., D. Hwang, K.-T. Yao, and Z. Yeh. 2006. "Mega-scale fabrication by contour crafting." *Int. J. Ind. Syst. Eng.* 1 (3): 301–320. https://doi.org/10.1504/IJISE.2006.009791.

Kira. 2015. "Winsun China builds world's first 3D printed villa and tallest 3D printed apartment building." Accessed February 27, 2019. https://www.3ders.org/articles/20150118-winsun-builds-world-first-3d-printed-villa-and-tallest-3d-printed-building-in-china.html.

Kounadis, A. 2015. "On the rocking-sliding instability of rigid blocks under ground excitation: Some new findings." *Soil Dyn. Earthquake Eng.* 75 (Aug): 246–258. https://doi.org/10.1016/j.soildyn.2015.03.026.

Kreiger, E., M. Kreiger, and M. Case. 2019. "Development of the construction processes for reinforced additively constructed concrete." *Addit. Manuf.* 28 (Aug): 39–49. https://doi.org/10.1016/j.addma.2019.02.015.

Labonnote, N., A. Rønnquist, B. Manum, and P. Rüther. 2016. "Additive construction: State-of-the-art, challenges and opportunities." *Autom. Constr.* 72 (Part 3): 347–366. https://doi.org/10.1016/j.autcon.2016.08.026.

Lagomarsino, S. 2015. "Seismic assessment of rocking masonry structures." *B. Earthquake Eng.* 13 (1): 97–128. https://doi.org/10.1007/s10518-014-9609-x.

Le, T., S. Austin, S. Lim, R. Buswell, A. Gibb, and T. Thorpe. 2012a. "Mix design and fresh properties for high-performance printing concrete." *Mater. Struct.* 45 (8): 1221–1232. https://doi.org/10.1617/s11527-012-9828-z.

Le, T., S. Austin, S. Lim, R. Buswell, R. Law, A. Gibb, and T. Thorpe. 2012b. "Hardened properties of high-performance printing concrete." *Cem. Concrete Res.* 42 (3): 558–566. https://doi.org/10.1016/j.cemconres.2011.12.003.

Lee, J., M. Park, H.-S. Lee, and H. Hyun. 2019. "Classification of modular building construction projects based on schedule-driven approach." *J. Constr. Eng. Manage.* 145 (5): 04019031. https://doi.org/10.1061/(ASCE)CO.1943-7862.0001656.

Levy, K. 2014. "A Chinese company 3-d printed 10 houses in a day." Accessed January 15, 2019. http://www.businessinsider.com/a-chinese-company-3d-printed-10-houses-in-a-day-2014-4.

Lim, S., R. Buswell, T. Le, S. Austin, A. Gibb, and T. Thorpe. 2012. "Developments in construction-scale additive manufacturing processes." *Autom. Constr.* 21 (1): 262–268. https://doi.org/10.1016/j.autcon.2011.06.010.

Lim, S., R. Buswell, P. Valentine, D. Piker, S. Austin, and X. De Kestelier. 2016. "Modelling curved-layered printing paths for fabricating large-scale construction components." *Addit. Manuf.* 12 (Part B): 216–230. https://doi.org/10.1016/j.addma.2016.06.004.

Liu, Y., D. Lu, Y. Wang, and H. Liu. 2016. "The sliding and overturning analysis of spent fuel storage rack based on dynamic analysis model." *Sci. Technol. Nucl. Installations* 2016 (4): 1–11. https://doi.org/10.1155/2016/8368504.

Lobaccaro, G., A. Wiberg, G. Ceci, M. Manni, N. Lolli, and U. Berardi. 2018. "Parametric design to minimize the embodied GHG emissions in a ZEB." *Energy Build.* 167 (May): 106–123. https://doi.org/10.1016/j.enbuild.2018.02.025.

Downloaded from ascelibrary.org by Alejandro Martínez Rocamora on 03/01/20. Copyright ASCE. For personal use only; all rights reserved.

Luo, Z., M. Wang, S. Wang, and P. Wei. 2008. "A level set-based parameterization method for structural shape and topology optimization." *Int. J. Numer. Methods Eng.* 76: 1–26. https://doi.org/10.1002/nme.2092.

Ma, G., and L. Wang. 2017. "A critical review of preparation design and workability measurement of concrete material for largescale 3D printing." *Front. Struct. Civ. Eng.* 12 (3): 382–400. https://doi.org/10.1007/s11709-017-0430-x.

Ma, G., L. Wang, and Y. Ju. 2018. "State-of-the-art of 3D printing technology of cementitious material—An emerging technique for construction." *Sci. China Technol. Sci.* 61 (4): 475–495. https://doi.org/10.1007/s11431-016-9077-7.

Malaeb, Z., H. Hachem, A. Tourbah, T. Maalouf, N. El Zarwi, and F. Hamzeh. 2015. "3D concrete printing: Machine and mix design." *Int. J. Civ. Eng. Technol.* 6 (6): 14–22.

Martabid, J., and C. Mourgues. 2015. "Criteria used for selecting envelope wall systems in Chilean residential projects." *J. Constr. Eng. Manage.* 141 (12): 05015011. https://doi.org/10.1061/(ASCE)CO.1943-7862.0001025.

Martens, P., M. Mathot, and F. Bos. 2018. "Optimising 3D printed concrete structures using topology optimisation." In Vol. 2 of *Proc., High Tech Concrete: Where Technology and Engineering Meet*. Cham, Switzerland: Springer.

Ostwald, M. 2010. "Ethics and the auto-generative design process." *Build. Res. Inf.* 38 (4): 390–400. https://doi.org/10.1080/09613218.2010.481172.

Panda, B., S. Paul, N. Mohamed, Y. Tay, and M. Tan. 2018. "Measurement of tensile bond strength of 3D printed geopolymer mortar." *J. Int. Meas. Conf.* 113 (Jan): 108–116. https://doi.org/10.1016/j.measurement.2017.08.051.

Paoletti, I. 2017. "Mass customization with additive manufacturing: New perspectives for multi performative building components in architecture." *Procedia Eng.* 180: 1150–1159. https://doi.org/10.1016/j.proeng.2017.04.275.

Peña, F., P. Lourenço, and A. Campos-Costa. 2008. "Experimental dynamic behavior of free-standing multi-block structures under seismic loadings." *J. Earthquake Eng.* 12 (6): 953–979. https://doi.org/10.1080/13632460801890513.

Perrot, A., D. Rangeard, and A. Pierre. 2016. "Structural built-up of cement-based materials used for 3D-printing extrusion techniques." *Mater. Struct.* 49 (4): 1213–1220. https://doi.org/10.1617/s11527-015-0571-0.

Raspall, F. 2015. "A procedural framework for design to fabrication." *Autom. Constr.* 51: 132–139. https://doi.org/10.1016/j.autcon.2014.12.003.

Reinoso, E., M. Jaimes, and L. Esteva. 2010. "Seismic vulnerability of an inventory of overturning objects." *J. Earthquake Eng.* 14 (7): 1008–1021. https://doi.org/10.1080/13632460903527971.

Shie, R., K. Ting, J. Yu, and C. Liu. 2007. "The sliding and overturning analysis of a free-standing cask under earthquake." *Solid State Phenomen.* 120: 207–212. https://doi.org/10.4028/www.scientific.net/SSP.120.207.

Tay, Y., B. Panda, S. Paul, N. Noor Mohamed, M. Tan, and K. Leong. 2017. "3D printing trends in building and construction industry: A review." *Virtual Phys. Prototyping* 12 (3): 261–276. https://doi.org/10.1080/17452759.2017.1326724.

Weng, Y., B. Lu, M. Tan, and S. Quian. 2016. "Rheology and printability of engineered cementitious composites-a literature review." In *Proc., 2nd Int. Conf. on Progress in Additive Manufacturing*, 427–432. Singapore: Nanyang Technological Univ.

Wolfs, R. 2015. "3D printing of concrete structures." Ph.D. thesis, Dept. of the Built Environment, Eindhoven Univ. of Technology.

Wu, P., J. Wang, and X. Wang. 2016. "A critical review of the use of 3-d printing in the construction industry." *Automat. Constr.* 68 (Aug): 21–31. https://doi.org/10.1016/j.autcon.2016.04.005.

Yhnova. 2018. "A house built in a matter of days by 3D printing thanks to the Batiprint3D method." Accessed January 15, 2019. http://batiprint3d.fr/wp-content/uploads/2017/10/NM_YHNOVA_DossierPresse_GB_09-17.pdf.

Zareiyan, B., and B. Khoshnevis. 2017a. "Effects of interlocking on interlayer adhesion and strength of structures in 3D printing of concrete." *Automat. Constr.* 83 (Nov): 212–221. https://doi.org/10.1016/j.autcon.2017.08.019.

Zareiyan, B., and B. Khoshnevis. 2017b. "Interlayer adhesion and strength of structures in contour crafting—Effects of aggregate size, extrusion rate, and layer thickness." *Automat. Constr.* 81 (Sep): 112–121. https://doi.org/10.1016/j.autcon.2017.06.013.

Downloaded from ascelibrary.org by Alejandro Martínez Rocamora on 03/01/20. Copyright ASCE. For personal use only; all rights reserved.